Histol Histopathol (2020) 35: 39-46

http://www.hh.um.es

Histology and Histopathology
From Cell Biology to Tissue Engineering

Microvascular pathology in Friedreich cardiomyopathy

Arnulf H. Koeppen[1,2], Jiang Qian[2], Alicia M. Travis[1], Alyssa B. Sossei[1], Paul J. Feustel[3] and Joseph E. Mazurkiewicz[3]

[1]Research Service, Veterans Affairs Medical Center, [2]Department of Pathology, Albany Medical Center and [3]Department of Neurosciences and Experimental Therapeutics, Albany Medical College, Albany, New York, USA

Summary. Heart disease is an integral part of Friedreich ataxia (FA). In addition to cardiomyocyte hypertrophy, fiber necrosis, and inflammatory infiltration, sections show fibrosis and disorganized capillaries. We examined the left ventricular wall (LVW) of 41 homozygous and 2 compound heterozygous FA patients aged 10-87 and 21 controls aged 2-69. Immunohistochemistry with an antibody to CD34 allowed quantitative counts of capillary profiles for a comparison with cardiomyocyte counts in the same field. Capillary counts (mean±standard deviation [SD]) in normal controls were 1926±341/mm^2, while mean cardiomyocyte counts were 2003±686/mm^2. The median ratio of capillaries to cardiomyocytes was 1.0 (interquartile range [IQR]: 0.9-1.2). In FA, the number of cardiomyocytes/mm^2 was significantly less (704±361; $p<0.001$), and the median ratio of capillaries to heart fibers was 2.0 (IQR:1.4-2.4). There was a significant correlation of the expanded guanine-adenine-adenine trinucleotides (shorter allele, GAA1) with a younger age of onset, shorter disease duration, and lower cardiomyocyte counts. The ratio of capillaries to heart fibers was higher in patients with long GAA1 repeat expansions (e.g., 3.31 in GAA1 of 1200). Double-label immunofluorescence for CD34 and the fibroblast marker S100A4 revealed co-expression in endothelial cells, supporting endothelial-to-mesenchymal transition in the pathogenesis of cardiac fibrosis in FA. We propose that the pathogenesis of FA heart disease includes primary fibrosis.

Offprint requests to: Arnulf H. Koeppen, MD, Research Service (151), VA Medical Center, 113 Holland Ave, Albany, NY 12208, USA. e-mail: arnulf.koeppen@med.va.gov

DOI: 10.14670/HH-18-132

Key words: Friedreich ataxia, Cardiomyopathy, Capillaries, Endothelial-to-mesenchymal transition, Fibrosis

Introduction

In his detailed clinical and pathological descriptions, Friedreich (1863, 1877) revealed that he was aware of heart disease but attributed cardiomyopathy to typhoid, presumably high fever toward the end of his patients' lives. Eighty-three years later, Russell (1946) recognized Friedreich cardiomyopathy as an integral part of the primarily neurological disease and described the lesion as myocarditis. More recent clinical reviews of Friedreich ataxia (FA) (Harding, 1981; Dürr et al., 1996; Weidemann et al., 2013; Corben et al., 2014) concluded that heart disease is very common and a frequent cause of death. Tsou et al. (2011), reported cardiomyopathy (defined as heart failure and arrhythmia) in 59% of all fatal outcomes. In a retrospective analysis of 30 autopsy cases of FA, Koeppen (2011) reported cardiac hypertrophy in 25 (83.3%).

The pathological phenotype of FA heart disease includes cardiomegaly, concentric hypertrophy, fiber necrosis, endomysial fibrosis, and focal inflammation. The enlargement of the heart is due to hypertrophy of individual heart fibers and fibrosis (Koeppen et al., 2015). The intercalated discs of the myocardium undergo widening, fragmentation, and chaotic disorganization (Koeppen et al., 2016). An intriguing observation is the presence of tiny iron-reactive granules in some cardiomyocytes (Lamarche et al., 1980; Michael et al., 2006), but there is no true cardiac iron overload in

the hearts of FA patients (Lamarche et al., 1980; Michael et al., 2006). Invariably, the cardiac lesion is more severe in the wall of the left ventricle, including the ventricular septum, but right ventricular wall, atria, and the cardiac conduction system are also affected. FA heart disease lends itself to the formation of mural thrombi, and embolism to brain, kidneys, and the large arteries of the extremities is common. Fibrosis of the heart is not solely due to scarring at sites of heart fiber necrosis. A mechanism that has not been studied before is endothelial-to-mesenchymal transition (endoMT), by which endothelial cells contribute to cardiac fibrosis. EndoMT can be detected by double-label immunofluorescence of CD34, a marker of endothelial cells, and S100A4, a fibroblast-specific marker.

Materials and methods

The Institutional Review Board of the Veterans Affairs Medical Center in Albany, NY, USA has approved the research that is described in this article. The autopsy specimens were obtained by a nationwide tissue donation program. Forty-three hearts were harvested from 41 FA patients with pathogenic homozygous guanine-adenine-adenine (GAA) trinucleotide repeat expansions and 2 patients with compound heterozygous mutations. Ages ranged from 10-87 years (mean± standard deviation [SD], 39±20). Disease duration was 4-68 years (28±15). In the homozygous patients, the GAA trinucleotide repeat expansion on the shorter allele (GAA1) ranged from 120 to 1200 (647±202). The longer allele (GAA2) was 170 to 1200 repeats (820±219). The two compound heterozygous patients had inherited their GAA expansions from their mothers (744 and 825, respectively). The other allele in both patients derived from their fathers and consisted of non-identical deletions in exon V of the frataxin gene (Becker et al., 2017).

Nine normal control hearts came from National Disease Research Interchange, Philadelphia, PA, and twelve from the autopsy practice of Albany Medical College, Albany, NY. In 6 of the 43 FA autopsy cases, prosectors did not record the fresh heart weights. In the remaining 37 cases, heart weights ranged from 279 to 662 g (413±89). The ages of the normal controls ranged from 2-69 years (median, 51 years, interquartile range [IQR] 26.5-60.5). On a non-parametric Mann-Whiney test, FA and control ages were not significantly different (p=0.255). Heart weights in the normal controls ranged from 60 to 525 g (315±123; significantly lower than FA by t-test, p=0.0033, and Mann-Whitney test, p=0.003). Detailed clinical information was available for all FA patients and controls. The diagnosis of FA cardiomyopathy was based on the pathological phenotype that included cardiomyocyte hypertrophy, fibrosis, and iron-reactive perinuclear granules in heart fibers. Based on the microscopic findings, 36 of 43 FA patients had cardiomyopathy (83.7%). Forty FA heart specimens displayed concentric hypertrophy. Only one case revealed dilatation of the right ventricle. Seven patients did not have cardiomyopathy as defined above. Heart failure and arrhythmia were recorded on hospital charts as primary or contributing causes of death in 26 FA patients (60.5%). Other causes of death were pneumonia (2), lung cancer (1), renal failure (1), myoglobinuria with renal failure (1), stroke (3), myocardial infarction (1), and chronic obstructive lung disease (1). Malnutrition and cachexia were the cause of death in 7 FA patients. These 7 deaths were attributed to the neurological disability of the patients. Ten FA patients had diabetes mellitus (23%). The causes of death in the 21 control patients were renal failure (1), liver failure (1), cancer of pancreas (1), breast (2), lung (1), colon (1), and esophagus (1), leukemia (3), disseminated Kaposi sarcoma (1), glioblastoma multiforme (1), purulent meningitis (1), septic shock (1), peritonitis (1), pulmonary embolism (2), aspiration pneumonia (1), abdominal trauma (1), and craniocerebral trauma (1).

Immunohistochemistry and double-label immunofluorescence

To visualize capillaries, 6 μm-thick paraffin sections of the left ventricular wall (LVW) of the heart were rehydrated and oxidized in methanol containing 3% hydrogen peroxide. Antigen retrieval consisted of the application of diluted "DIVA" (1:10) for 30 min at 95°C and gradual cooling to room temperature (RT). DIVA is a proprietary preparation of Biocare Medical (Pacheco, CA, USA; cat. No. DV2004MX). The next step was "suppression" of non-specific antibody binding by incubation at RT in 10% normal horse serum (by volume [vol]) and 0.5% bovine serum albumin (BSA) (by weight/vol) in phosphate-buffered saline (PBS). Capillaries were visualized by immunohistochemistry with mouse monoclonal anti-CD34 (0.8 μg protein/ml; Santa Cruz Biotechnology, Dallas, TX, USA; cat. No. sc-74499) in PBS containing 1% normal horse serum and 0.5% BSA (overnight at 4°C). After removal of the antibody by repeated washing with PBS, the sections were incubated for 2 hours (h) at RT in biotinylated goat anti-mouse IgG (1 μg/ml; Vector Laboratories, Burlingame, CA; cat. No. BA-9200). The sections were then incubated for 1h at RT in horseradish-peroxidase-labeled streptavidin (1 μg/ml; Sigma-Aldrich, St. Louis, MO, USA; cat. No. S5512). Reaction product was generated with a solution of diaminobenzidine (0.7 mg/ml) and urea-hydrogen peroxide (2 mg/ml) (Sigma; cat. No. D4168). Slides were counterstained with diluted brazilin (1:10; Anatech, Battle Creek, MI, USA; cat. No. 861), dehydrated through a series of ethanol and xylene, and cover-slipped by standard methods.

For the visualization of cardiac fibroblasts, rabbit polyclonal anti-S100A4 (1 μg protein/ml; Invitrogen, Rockford, IL, USA; cat. No. PA5-16586) replaced anti-CD34, and the secondary antibody was biotinylated goat anti-rabbit IgG (1 μg/ml; Vector Laboratories; cat. No. BA-1000). Other immunohistochemical steps were

identical to those for CD34. Slides stained for S100A4 were not counterstained.

To assess endoMT, CD34 and S100A4 were visualized on the same slide by double-label immunofluorescence with the respective antibodies. Slide preparation was similar to immunohistochemistry, including antigen retrieval by DIVA, but oxidation in hydrogen peroxide-methanol was omitted. The principal steps were described in a previous publication from this laboratory (Koeppen et al., 2017). Fluorescence of one member of the pair was enhanced by insertion of an amplifying step, as follows: After overnight incubation with the primary antibody, sections intended for the display of CD34 were incubated for 2h at RT in biotinylated anti-mouse IgG. For comparable enhancement of S100A4 fluorescence, the amplification was by biotinylated anti-rabbit IgG. Only one of the antigen-antibody reactions was amplified. After washing in PBS, the sections were overlaid with Alexa Fluor 488-labeled streptavidin (Jackson ImmunoResearch, West Grove, PA, USA; cat. No. 016-540-084; 0.45 μg/ml) (for CD34) or Cy3-labeled donkey anti-rabbit IgG (Jackson ImmunoResearch; cat. No. 711-165-152; 0.375 μg/ml) (for S100A4). After 4h, the sections were washed in PBS and cover-slipped under 50% ultrapure glycerol in PBS. Sections were viewed in a Zeiss LSM 880 laser confocal scanning microscope. Images were collected through the band passes of 507-544 nm for Alexa Fluor 488 (CD34) and 568-631 nm for Cy3 (S100A4).

Quantitative analysis

Sections stained for CD34 and counterstained with brazilin were examined in a Zeiss Axiophot microscope equipped with a digital camera and an AxioVision SE64 program. Fields of 0.15 mm^2 were selected to display transversely cut cardiomyocytes. The program allowed counting of heart fibers and capillaries. When capillaries were connected by lateral branches, only one vessel was counted. Capillary profiles were labeled by black crosses to prevent accidental duplicate recording. Cardiomyocytes were counted and marked by green crosses (Fig. 2). Counts of 5 non-overlapping fields were averaged and expressed as counts/mm^2. This procedure yielded the numerical abundance of capillaries and cardiomyocytes per unit area in identical fields from which the ratios of capillaries/cardiomyocytes were calculated. Additional analytical steps were the correlation of capillary and cardiomyocyte counts, and the capillary/cardiomyocyte ratios, with the ages of the patients, and a three-dimensional scatter plot of the ratio *vs*. age and GAA1 trinucleotide repeats (homozygous FA patients only). Statistical comparisons were made using subject mean value as one experimental unit. Means and SD are reported with statistical inference by Student's independent sample t-test. Correlations were examined using multiple linear regression. Minitab 18 (State College, PA, USA) statistical software was used with significance accepted at the 0.05 level.

Results

Figure 1 shows distribution and extent of cardiac fibrosis in FA cardiomyopathy (Fig. 1D) and the disorganization of capillaries (Fig. 1E,F). On longitudinal sections of normal LVW, capillaries run alongside cardiomyocytes over some distance, and anastomotic connections between the vessels are

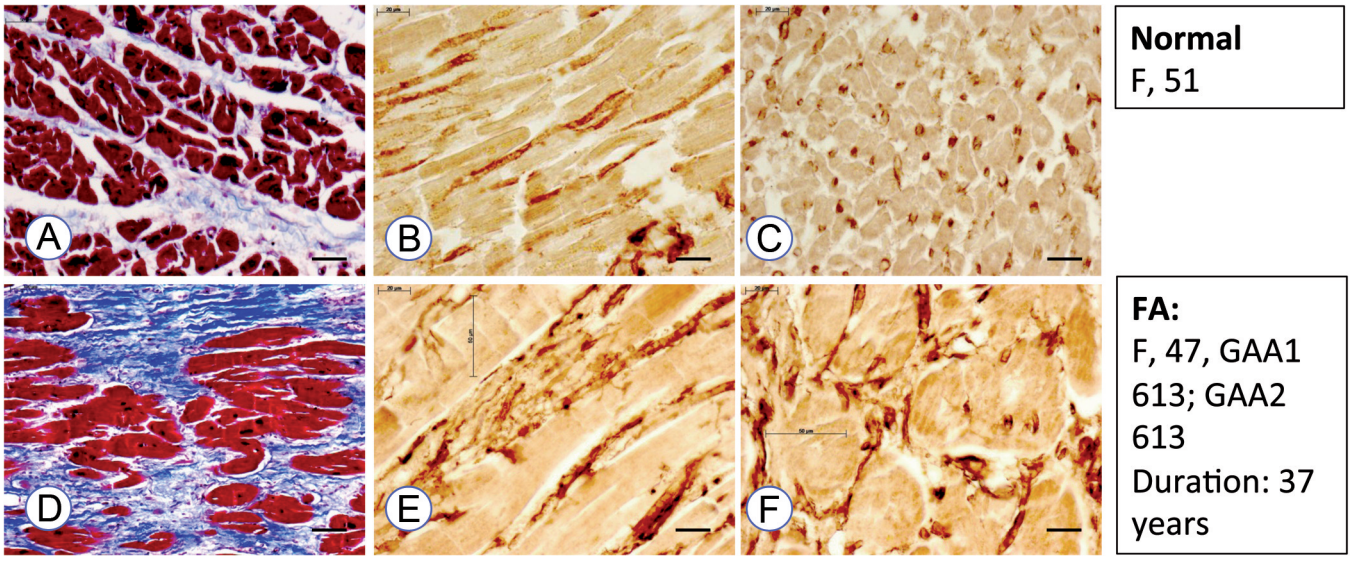

Fig. 1. Fibrosis and capillaries in FA cardiomyopathy. **A-C.** 51-year-old normal female control. **D-F.** 47-year-old woman with FA. GAA1=613; GAA2=613. Stains: **A** and **D**, trichrome; **B, C, E**, and **F**, CD34 immunohistochemistry. The myocardium in FA **(D)** shows extensive fibrosis that is both focal and diffuse. The capillaries in FA are hyperplastic and disorganized **(E, F)** compared to the regular parallel alignment along cardiomyocytes in the control case **(B, C)**. In FA, heart fibers are hypertrophic **(E, F).** Scale bars: 20 μm; thin bars E, F, 50 μm.

uncommon (Fig. 1B). In contrast, capillaries of the LVW in FA appear disorganized, and anastomoses are frequent (Fig. 1E,F). Figure 2 illustrates how capillaries and cardiomyocytes were counted in identical microscopic fields. We did not consider blood vessels that were recognizable as arterioles.

At first glance, capillary profiles in FA cardiomyopathy appear more abundant than normal, but a systematic analysis reveals numerical reduction of capillary profiles per one mm^2 (Fig. 3) ($p<0.001$; t-test). While anti-CD34 gave the most robust visualization of capillary walls, immunohistochemistry with antibodies to CD31 or vascular endothelial growth factor, and lectin affinity histochemistry with biotinylated Ricinus communis agglutinin generated a similar result, namely, of numerically reduced capillary profiles/mm^2 in FA (not illustrated).

Longitudinal and cross sections of LVW in FA also confirmed the known cardiomyocyte hypertrophy in FA (Fig. 1E,F) (Koeppen et al., 2015), and this process reduced the number of fibers that could be accommodated in the standard microscopic field of 0.15 mm^2. Figure 4 shows the distribution of cardiomyocytes in FA and control LVW, revealing the lower count of heart fibers/mm^2 in FA ($p<0.001$; t-test). The ratio of capillary to cardiomyocytes counts, however, rises steeply in FA ($p<0.001$; t-test). In normal LVW, it is near 1 (Fig. 5). In other words, in control hearts, the number of capillaries/mm^2 equals that of cardiomyocytes, but in FA, capillaries outnumber heart fibers. The correlation of cardiomyocyte counts/mm^2 with the age of the patients shows only limited change in FA (Fig. 6) whereas normal young persons have a much larger number of heart fibers/mm^2. The well-known effect of short pathogenic GAA1 trinucleotide repeats on the neurological FA phenotype is also apparent in the

Fig. 2. Quantitative counts of capillaries and cardiomyocytes in LVW of a normal control. Capillary endothelium was stained with anti-CD34. The counter stain, brazilin, was used to identify heart fibers. Capillaries were marked by black crosses **(B)**, cardiomyocytes by green crosses **(C)**. The microscopic field measured 0.15 mm^2. After averaging the counts in five non-overlapping fields of identical size, the mean number of capillaries/mm^2 was 1540, the mean number of cardiomyocytes, 1253, yielding a capillary-to-cardiomyocyte ratio of 1.23. Scale bars: 50 μm.

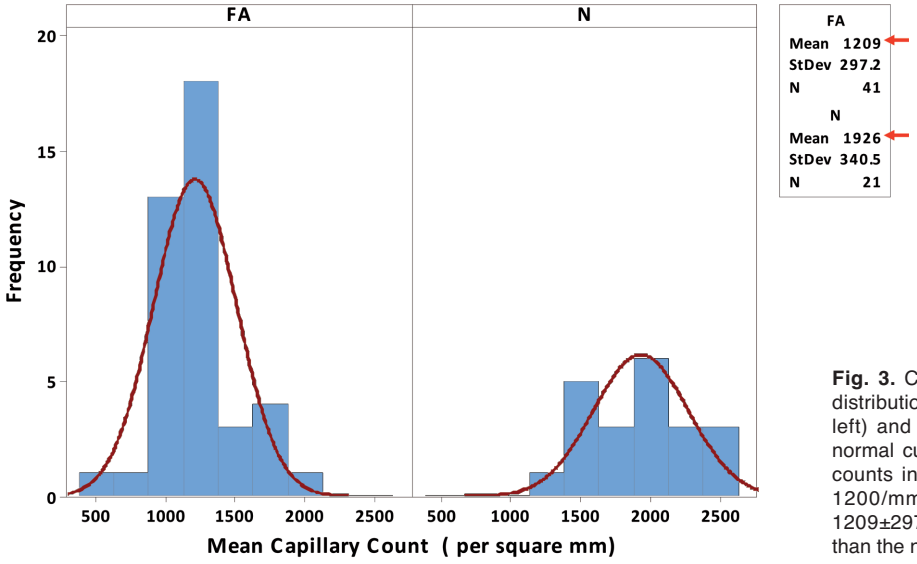

Fig. 3. Capillary deficit in FA. Histograms display the distribution of capillary counts/mm^2 in FA patients (FA, left) and normal controls (N, right) with overlaid fitted normal curves. In FA, the distribution of mean capillary counts in 41 homozygous FA patients clusters around 1200/mm^2. Mean±SD of all measurements in FA is 1209±297, which is significantly less ($p<0.001$; t-test) than the normal values of 1926±341.

analysis of the microvascular pathology of the heart (Fig. 7). In patients with long GAA1 repeats and FA onset at a young age, the ratio of capillaries to cardiomyocytes is very high. In a patient with short GAA1 trinucleotide repeats, e.g. 200 (right lower arrow in Fig. 7), death occurred at age 76, and the ratio of capillaries to heart fibers was in the normal range (near 1) (Fig. 7).

Figure 8A-C display the immunohistochemical results with anti-S100A4. In Fig. 8A, a capillary of the LVW of an FA patient is fully ensheathed by fibroblasts. In two other patients with FA, processes of fibroblast lie near blood vessels (Fig. 8B,C). Strongly S100A4-reactive fibroblasts in normal endomysium are uncommon (not illustrated). Figure 8D-F illustrate the co-expression of CD34 and S100A4 by double-label immunofluorescence of LVW in an FA patient.

Discussion

Abnormal myocardial capillaries in FA

The static anatomical observations on capillaries in the LVW of FA patients (Fig. 2) do not allow direct conclusions about the effect of the disease on blood flow. Fig. 1E,F suggest that capillaries in FA are hyperplastic, but the reduced number of vessels/mm^2 is likely due to hypertrophy of cardiomyocytes that

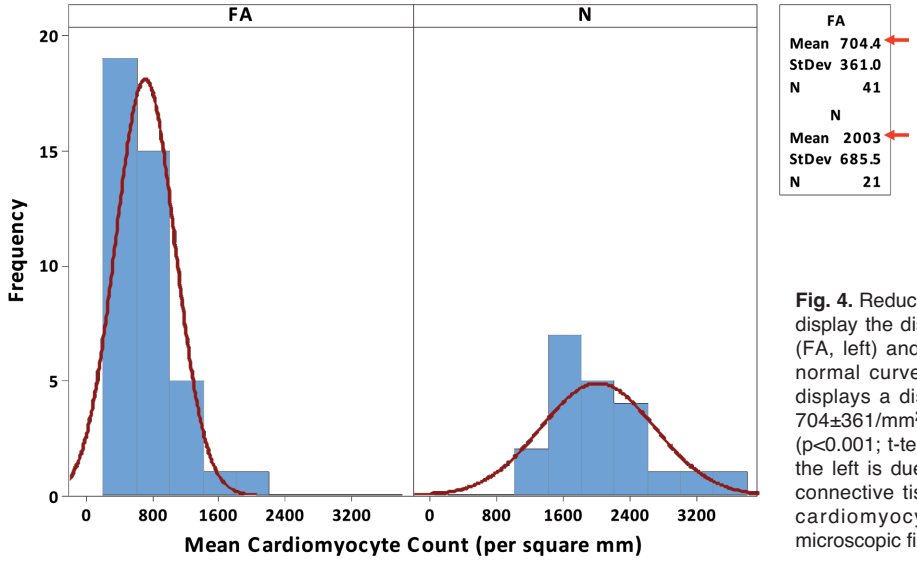

Fig. 4. Reduced number of cardiomyocytes in FA. Histograms display the distribution of cardiomyocytes/mm^2 in FA patents (FA, left) and normal controls (N, right) with overlaid fitted normal curves. The numerical distribution of heart fibers displays a distinct shift to the left in FA. The mean±SD is 704±361/mm^2. The normal controls show more fibers/mm^2 ($p<0.001$; t-test) with mean±SD being 2003±686. The shift to the left is due to fiber hypertrophy and the accumulation of connective tissue, reducing the number of cross-sectioned cardiomyocytes that could be accommodated by the microscopic field.

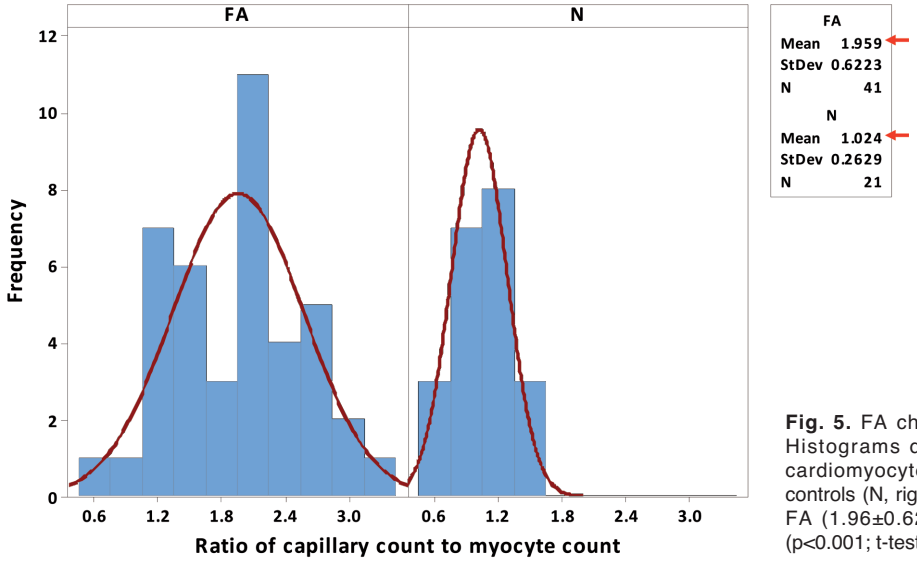

Fig. 5. FA changes the capillary-to-cardiomyocyte ratio. Histograms display the distribution of the capillary-to-cardiomyocyte ratio in FA patients (FA, left) and normal controls (N, right). The ratio of capillaries to cardiomyocytes in FA (1.96±0.622) is statistically significantly higher in FA ($p<0.001$; t-test) than in the normal controls (1.024±0.263).

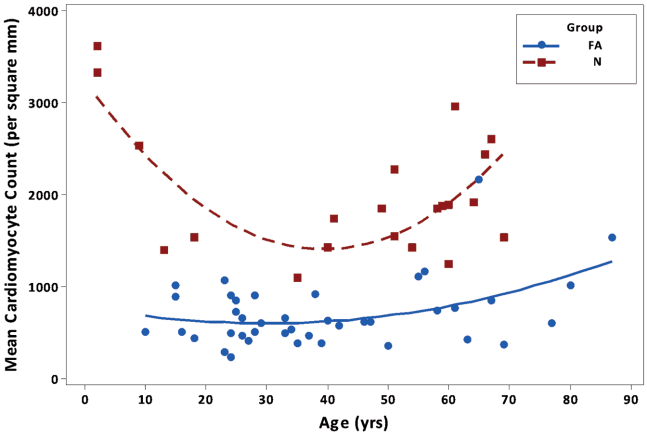

Fig. 6. Regression of cardiomyocytes as a function of age. The curve for FA shows only modest changes in the heart fiber counts/mm^2 between very young and old patient ages. In contrast, young normal persons (N) have a much higher fiber density that declines with aging. A quadratic term was used in the multiple linear regression to model the curvature.

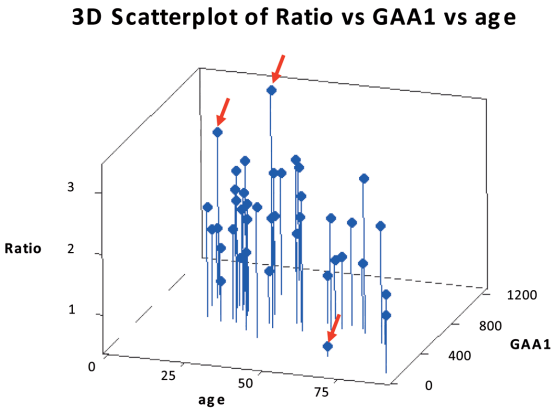

Fig. 7. Three-dimensional scatterplot of capillary-to-cardiomyocyte ratios vs GAA1 vs age in 41 homozygous FA patients. The illustration highlights the effect of the GAA1 trinucleotide repeat expansion on the age of death and the capillary-to-cardiomyocyte ratio. A long expansion, such as shown by the top red arrow correlates with short survival and a high capillary/cardiomyocyte ratio. Short GAA1 expansions, such as shown by the lower right arrow, correlate with long survival and a normal capillary-to-cardiomyocytes ratio. The arrow to the left of the top arrow shows a premature death in a patient with a high capillary-to-cardiomyocyte ratio and a moderate GAA1 expansion.

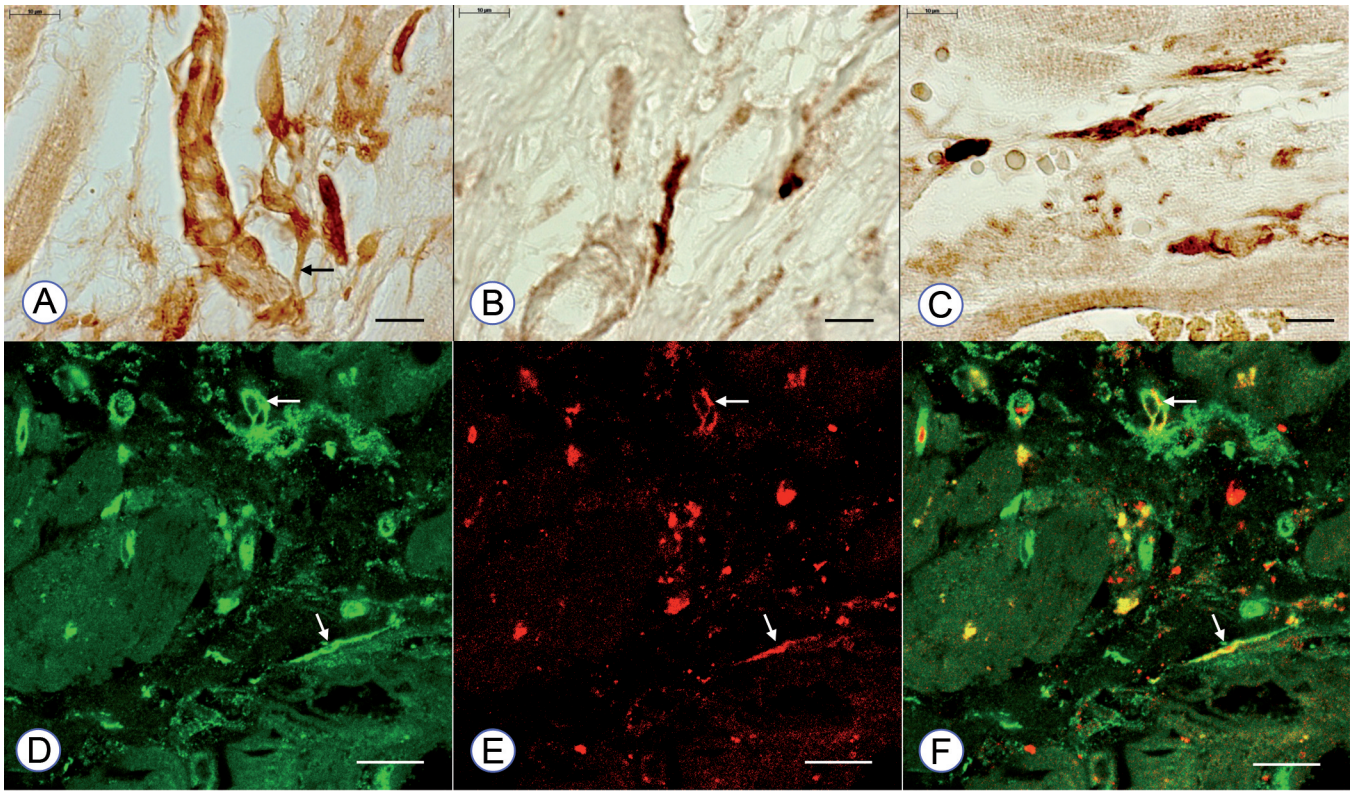

Fig. 8. EndoMT in FA. **A-C.** Immunohistochemistry with anti-S100A4: female FA patient **(A)**, 47, GAA1, 613, GAA2, 613; male **(B, C)**, 46, GAA1, 599; GAA2 599; Double-label immunofluorescence of CD34 **(D-F)** (**D**, Alexa Fluor 488, green) and S100A4 (**E**, Cy3, red)**. F.** Merged images of **D** and **E**. Male **(D-F)**, 28, GAA1, 528, GAA2, 911. In **(A)**, S100A4-reactive fibroblasts surround a capillary, and one fibroblast extends a process toward the vessel (arrow) the vessel walls. **(D-F)** show the colocalization of CD34 and S100A4 in the endothelium of some capillaries (arrows).

displaces the adjacent capillaries so that their total number per unit area (mm^2) is significantly lower than normal (Fig. 3).

Capillary blood flow through the myocardium is a complex process and involves arterial pressure in the coronary arteries, hemodynamic pressure in the coronary sinus, osmotic pressure in the circulating plasma, osmotic and hydrostatic pressures in the interstitial space of the heart, and lymphatic drainage (Dongaonkar et al., 2010). It is of interest that during systole, the vigorous contraction of cardiac muscle compresses myocardial capillaries and temporarily interrupts flow. Therefore, myocardial perfusion is generally measured during end diastole, and a myocardial perfusion reserve index may be determined by magnetic resonance imaging (MRI) after signal enhancement with gadolinium and adenosine-induced heart stress (Cerqueira et al., 2002; Cook et al., 2009). Raman et al. (2011), observed impaired myocardial perfusion reserve in 26 FA patients. The location of the reduced end-diastolic signal in FA was between endo- and epicardium, corresponding to the cross sections of the LVW in this report.

Scarring or primary fibrosis in FA cardiomyopathy

In addition to hypertrophy, cardiomyocytes in FA cardiomyopathy undergo frank necrosis and invasion by macrophages. It is reasonable to attribute focal scarring to proliferation of resident fibroblasts or precursors recruited from the circulation. Russell (1946) called the progressive fiber destruction in FA "piecemeal" and thought that loss of contractile tissue was responsible for hypertrophy of neighboring cardiomyocytes. She did not specifically express an opinion on scarring vs diffuse fibrosis. Beyond scarring at sites of heart fiber necrosis, FA hearts are also affected by more diffuse fibrosis, which may be due to endoMT.

The transition of cardiac endothelial cells to mesenchymal cells is a critical step in the normal formation of heart valves (Eisenberg and Markwald, 1995) and sealing of the foramen ovale (Elliott et al., 2014). The molecular events underlying endoMT in pathological cardiac fibrosis have been analyzed mostly in rodents (Zeisberg et al., 2007; Goumans et al., 2008; Piera-Velazquez et al., 2011; Wermuth et al., 2016) while human hearts have not been systematically examined. The critical cytokine in the initiation of endoMT is transforming growth factor β1 (TGF-β1) (Zeisberg et al., 2007) though downstream signaling to endoMT involves multiple other proteins and genes (Goumans et al., 2008; Widyantoro et al., 2010; Piera-Velazquez et al., 2011). In the living animal, the induction of endoMT by TGF-β1 can be blocked by systemic administration of recombinant human bone morphogenetic protein 7 (rhBMP-7). Piera-Velazquez et. al. (2011) reviewed endoMT in experimental animals and estimated that 27-35% of cardiac fibroblasts derive from endoMT. Reliable animal models of cardiac fibrosis are the induction of diabetes mellitus and aortic banding, or induction of diabetes in spontaneously hypertensive rats. It is unknown whether endoMT in human hearts is a similar contributor to cardiac fibrosis in FA or other diseases. The FA patients whose heart sections are illustrated in Fig. 8 did not have diabetes mellitus, and it remains unsettled whether the coexistence of FA and diabetes mellitus is important in endoMT and cardiac fibrosis.

Emerging therapy of fibrosis in FA cardiomyopathy

An effective therapy for heart disease in FA does not exist. It is unlikely that systemic administration of rhBMP-7 will become a practical treatment of cardiac fibrosis in FA or other human fibrotic disorders. Drug therapy with angiotensin II-receptor blockers (Tang et al., 2013; Wu et al., 2016) reversed cardiac fibrosis in diabetic rats and improved cardiac function on echocardiography. The profibrotic properties of angiotensin II have been known for some time (review in Kurdi and Booz, 2011). While this research paper does not provide conclusive evidence for the reversibility of cardiac fibrosis in FA, angiotensin II-receptor blockers may be promising in a clinical trial with FA patients who have heart disease.

Limitations

A critical challenge in the interpretation of gross and microscopic observations on FA heart tissues obtained at autopsy is the correlation with the progression of the disease during life. There is no doubt that FA heart disease progresses, and autopsy studies may not be fit to look back at the time between FA onset and death. Tissue samples obtained from FA patients with a wide spectrum of disease duration (4-68 years), however, may provide clinicoanatomic correlations. An early death equals rapid progression, and death at advanced age is equivalent to a more benign disease course. While S100A4 is a suitable marker for fibroblasts and is often called the "fibroblast-specific protein" (review in Schneider et al., 2008), visualization of other fibrosis-related proteins, such as matrix metalloprotease 9, will be needed to confirm, and perhaps quantify the contribution of endoMT to the overall fibrotic state of hearts in FA.

Acknowledgements. The authors wish to thank the families that have allowed autopsies to advance research in Friedreich ataxia, and pathologists who harvested tissues, often under very difficult circumstances. National Disease Research Interchange receives support from the National Institutes of Health (grant number U42 OD0111158). The laboratory work was completed in the research facilities of the Veterans Affairs Medical Center, Albany, NY, USA, and the Department of Neurosciences and Experimental Therapeutics of Albany Medical College, Albany, NY, USA. This study was supported by a grant from Friedreich's Ataxia Research Alliance (to AHK).
Conflict of interest. The authors do not declare a conflict of interest

References

Becker A.B., Qian J., Gelman B.B., Yang M., Bauer P. and Koeppen A.H. (2017). Heart and nervous system pathology in compound heterozygous Friedreich ataxia. J. Neuropathol. Exp. Neurol. 76, 665-675.

Cerqueira M.D., Weissman N.J., Dilsizian V., Jacobs A.K., Kaul S., Laskey W.K., Pennell D.J., Rumberger J.A., Ryan T. and Verani M.S. (2002). Standardized myocardial segmentation and nomenclature for tomographic imaging of the heart. A statement for healthcare professionals from the Cardiac Imaging Committee of the Council on Clinical Cardiology of the American Heart Association. Circulation 105, 539-542.

Cook S.C., Ferketich A.K. and Raman S.V. (2009). Myocardial ischemia in asymptomatic adults with repaired aortic coarctation. Int. J. Cardiol. 133, 95-101.

Corben L.A., Lynch D., Pandolfo M., Schulz J.B., Delatycki M.B. and the Clinical Management Guidelines Writing Group. (2014). Consensus clinical management guidelines for Friedreich ataxia. Orphanet J. Rare Dis. 9, 184.

Dongaonkar R.M., Stewart R.H., Geissler H.J. and Laine G.A. (2010). Myocardial microvascular permeability, interstitial oedema, and compromised cardiac function. Cardiovasc. Res. 87, 331-339.

Dürr A., Cossée M., Agid Y., Campuzano V., Mignard C., Penet C., Mandell J.L., Brice A. and Koenig M. (1996). Clinical and genetic abnormalities in patients with Friedreich's ataxia. New Engl. J. Med. 335, 1169-1175.

Eisenberg L.M. and Markwald R.R. (1995). Molecular regulation of atrioventricular valvuloseptal morphogenesis. Circ. Res. 77, 1-6.

Elliott G.C., Gurtu R., McCollum C., Newman W.G. and Wang T. (2014). Foramen ovale closure is a process of endothelial-to-mesenchymal transition leading to fibrosis. PLoS One 9, e107175.

Friedreich N. (1863). Ueber degenerative Atrophie der spinalen Hinterstränge. Virchows Arch. Pathol. Anat. Physiol. Klin. Med. 26, 391-419.

Friedreich N. (1877). Ueber Ataxie mit besonderer Berücksichtigung der hereditären Formen. Nachtrag (Postscriptum). Virchows Arch. Pathol. Anat. Physiol. Klin. Med. 70, 140-152.

Goumans M.J., van Zonneveld A.J. and ten Dijke P. (2008). Transforming growth factor β-induced endothelial-to-mesenchymal transition: A switch to cardiac fibrosis? Trends Cardiovasc. Med. 18, 293-298.

Harding A.E. (1981). Friedreich's ataxia: A clinical and genetic study of 90 families with an analysis of early diagnostic criteria and intrafamilial clustering of clinical features. Brain 104, 589-620.

Koeppen A.H. (2011). Friedreich's ataxia: Pathology, pathogenesis, and molecular genetics. J. Neurol. Sci. 303, 1-12.

Koeppen A.H., Ramirez R.L., Becker A.B., Bjork S.T., Levi S., Santambrogio P., Parsons P.J., Kruger P.C., Yang K.X., Feustel P.J. and Mazurkiewicz J.E. (2015). The pathogenesis of cardiomyopathy in Friedreich ataxia. PLoS One 10, e116396.

Koeppen A.H., Becker A.B., Feustel P.J., Gelman B.B. and Mazurkiewicz J.E. (2016). The significance of intercalated discs in the pathogenesis of Friedreich cardiomyopathy. J. Neurol. Sci. 367, 171-176.

Koeppen A.H., Becker A.B., Qian J., Gelman B.B. and Mazurkiewicz J.E. (2017). Friedreich ataxia: Developmental failure of the dorsal root entry zone. J. Neuropathol. Exp. Neurol. 76, 969-977.

Kurdi M. and Booz G.W. (2011). New take on the role of angiotensin II in cardiac hypertrophy and fibrosis. Hypertension 57, 1034-1038.

Lamarche J.B., Côté M. and Lemieux B. (1980). The cardiomyopathy of Friedreich's ataxia morphological observations in 3 cases. Can. J. Neurol. Sci. 7, 389-396.

Michael S., Petrocine S.V., Qian J., Lamarche J.B., Knutson M.D., Garrick M.D. and Koeppen A.H. (2006). Iron and iron-responsive proteins in the cardiomyopathy of Friedreich's ataxia. Cerebellum 5, 257-267.

Piera-Velazquez S., Li Z. and Jimenez S.A. (2011). Role of endothelial-mesenchymal transition (EndoMT) in the pathogenesis of fibrotic disorders. Am. J. Pathol. 179, 1074-1080.

Raman S.V., Phatak K., Hoyle J.C., Pennell M.L., McCarthy B., Tran T., Prior T.W., Olesik J. W., Lutton A., Rankin C., Kissel J.T. and Al-Dahhak R. (2011). Impaired myocardial perfusion reserve and fibrosis in Friedreich ataxia: a mitochondrial cardiomyopathy with metabolic syndrome. Eur. Heart J. 32, 561-567.

Russell D.S. (1946). Myocarditis in Friedreich's ataxia. J. Pathol. Bact. 63, 739-748.

Schneider M., Hansen J.L. and Sheikh S.P. (2008). S100A4: a common mediator of epithelial-mesenchymal transition, fibrosis and regeneration in diseases? J. Mol. Med (Berl). 86, 507-522.

Tang R.N., Lv L.L., Zhang J.D., Dai H.Y., Li Q., Zheng M., Ni J., Ma K.L. and Liu B.C. (2013). Effects of angiotensin II receptor blocker on myocardial endothelial-to-mesenchymal transition in diabetic rats. Int. J. Cardiol. 162, 92-99.

Tsou A.Y., Paulsen E.K., Lagedrost S.J., Perlman S.L., Mathews K.D., Wilmot G.R., Ravina B., Koeppen A.H. and Lynch D.R. (2011). Mortality in Friedreich ataxia. J. Neurol. Sci. 307, 46-49.

Weidemann F., Störk S., Liu D., Hu K., Herrmann S., Ertl G. and Niemann M. (2013). Cardiomyopathy of Friedreich ataxia. J. Neurochem. 126 (supp 1), 88-93.

Wermuth P.J., Li Z., Mendoza F.A. and Jimenez S.A. (2016). Stimulation of transforming growth factor-β1-induced endothelial-to-mesenchymal transition and tissue fibrosis by endothelin-1 (ET-1): A novel profibrotic effect of ET-1. PLoS One 11, e0161988.

Widyantoro B., Emoto N., Nakayama K., Anggrahini D.W., Adiarto S., Iwasa N., Yagi K., Miyagawa K., Rikitake Y., Suzuki K., Kisanuki Y.Y., Yanagisawa M. and Hirata K. (2010). Endothelial cell-derived endothelin-1 promotes cardiac fibrosis in diabetic hearts through stimulation of endothelial-to-mesenchymal transition. Circulation 121, 2407-2418.

Wu M., Peng Z., Zu C., Ma J., Lu S., Zhong J. and Zhang S. (2016). Losartan attenuates myocardial endothelial-to-mesenchymal transition in spontaneous hypertensive rats via inhibiting TGF-β/Smad signaling. PLoS One 11, e0155730.

Zeisberg E.M., Tarnavski O., Zeisberg M., Dorfman A.L., McMullen J.R., Gustafsson E., Chandraker A., Yuan X., Pu W.T., Roberts A.B., Neilson E.G., Sayegh M.H., Izumo S. and Kalluri R. (2007). Endothelial-to-mesenchymal transition contributes to cardiac fibrosis. Nat. Med. 13, 952-961.

Accepted June 5, 2019